Composite Structures 389 (2026) 120401

Contents lists available at ScienceDirect

Composite Structures

journal homepage: www.elsevier.com/locate/compstruct

Non-contact detection of interlaminar defects in titanium-graphite FMLs using laser ultrasonics and thermography

Nicola Montinaro [a,b,*], Gabriella Epasto [c], Donatella Cerniglia [a], Antonio Pantano [a]

[a] Department of Engineering, University of Palermo, Viale delle Scienze Ed.8, Palermo, Italy
[b] Institute for Advanced Energy Technologies "Nicola Giordano" (ITAE), National Research Council, Viale delle Scienze Edificio 9, Palermo 90128, Italy
[c] Dipartimento di Ingegneria, Università Degli Studi di Messina, Contrada di Dio, Sant'Agata, Messina 98166, Italy

ARTICLE INFO

Keywords:
Fibre Metal Laminate
Pulsed Thermography
Lamb waves
Hybrid composite structures
Guided ultrasonic waves
Ultrasonic imaging
Delamination

ABSTRACT

The use of fully non-contact Laser Ultrasonic Testing (LUT) for the inspection of advanced hybrid composites, such as Fiber Metal Laminates (FMLs), offers significant advantages for industrial applications. The LUT setup provides high flexibility, enabling the generation of multiple ultrasonic wave modes and access to difficult-to-reach areas without the need for surface preparation. However, the inherent heterogeneity of FMLs, characterized by multiple interfaces and contrasting material properties, presents challenges in wave propagation and signal interpretation, particularly due to the presence of Lamb waves. In this study, a LUT pitch-catch ultrasonic configuration was developed to inspect a 10-layers Ti-Gr laminate containing artificial defects. The system successfully identified flaws up to the fourth interface and enabled partial shape characterization up to the third. Rapid scanning via B-scan mapping and targeted high-resolution C-scans allowed efficient localization and detailed evaluation of defects. Results were validated through complementary pulsed thermography, confirming the reliability and robustness of the proposed inspection method.

1. Introduction

Fiber Metal Laminates (FMLs) are hybrid materials composed of alternating layers of metal and composite materials. Being lightweight one of the requested features, the metal layers are often made of Alluminium, such as in ARALL (Aramidic Reinforced ALLuminium), GLARE (GLass REinforced Alluminium) and CARALL (CArbon Reinforced ALLuminium), or of Titanium, as the FML used in this paper, Ti-Gr (Titanium Graphite) in which layers of titanium alternate with a carbon fiber composite. The fiber layers can also be made of natural fibers, such as flax, and/or mineral fibers, like basalt: both composition and stacking significantly affect the mechanical properties of the material [1].

The advantages of FMLs are: high strength-to-weight ratio, excellent fatigue resistance and higher damage tolerance, impact resistance, thermal insulation, and corrosion resistance, compared to traditional metals or composites alone [2–4]. Conversely, FMLs might exhibit some issues that affect performance and reliability: inclusions, voids, cracking and corrosion, delamination, fiber misalignment, and poor bonding.

This class of materials is primarily used in cutting-edge applications such as aerospace (e.g. large parts of the Airbus A320 fuselage are made of GLARE), military and motorsports. Their lightweight properties make them attractive to the marine, automotive, and aerospace industries [5]. Considering the uses of FMLs, ensuring the integrity of these structures throughout their life is crucial. The development of reliable, fully non-contact and easy-to-apply non-destructive testing (NDT), able to check the integrity of each layer of the laminate during manufacturing and afterwards in periodical inspections, is still a complex task. FMLs are affected by the same defects in traditional composites, such as carbon, Kevlar and glass-fiber-reinforced polymers; thus, even some of the inspection techniques used are the same: X-ray radiography, Eddy Current Testing, Acoustic Emission, Infrared Thermography (IRT) and Ultrasonic Testing (UT) [6–10]. Among all these techniques, this research is focused on UT, used as the primary technique, and IRT as a control and comparison. The most effective UT setups are usually water-coupled transmission C-scans (e.g. used for inspecting FMLs at FOKKER®). These approaches are not fast and are better suited for post-manufacturing quality checks, thanks to the easier handling and accessibility of components [11]. Ultrasonic Pulse-Echo, Ultrasonic Phased Array, and Eddy Currents have been found effective for in-service, single-side inspection of small cracks, porosities, and delaminations, but they are best suited for the quality check of small sites and less convenient for large areas [12,13]. Moreover, in thin FML structures, contact

* Corresponding author.
E-mail address: nicola.montinaro@unipa.it (N. Montinaro).

https://doi.org/10.1016/j.compstruct.2026.120401
Received 28 July 2025; Received in revised form 10 March 2026; Accepted 28 April 2026
Available online 2 May 2026

Nomenclature

LUT	Laser Ultrasonic Testing
FML	Fiber Metal Laminate
ARALL	Aramidic Reinforced ALLuminium
GLARE	GLass REinforced Alluminium
CARALL	CArbon Reinforced ALLuminium
Ti-Gr	Titanium Graphite
ACLU	Air-Coupled Laser Ultrasonic
IRT	InfraRed Thermography
UT	Ultrasonic Testing
CFRP	Carbon Fibre Reinforced Plastic
FBH	Flat Bottom Holed
S_n	Symmetrical Ultrasonic wave of the n-order
A_n	Anti-symmetrical Ultrasonic wave of n-order
PT	Pulsed Thermography
FEP	Fluorinated Ethylene Propylene
IR	Infrared Wave
MW	Mid-Wave infrared
CW	Continuous Wave Laser Beam
IFOV	Instant Field Of View
S-R	Source-Receiving distance
PPT	Pulsed Phase Thermography

UT techniques do not allow the generation of far-field and detection of reflected waves; thus, only water/air-coupled and fully non-contact UT are feasible for defect detection. Jakubczak et al. [14] found that phased array techniques are capable of detecting damage in FML, especially through transmission phased array, which is more effective in assessing the conditions of hybrid laminates than conventional UT. Wang et al. [15] proved that a high-resolution and highly sensitive Air-Coupled Laser Ultrasonic (ACLU) system can detect debonding on curved Al/CFRP interface, detect air pockets trapped between Al and CFRP, and locate the damage regions. Phased-array ultrasonic and digital radiography images were used to demonstrate the high resolution and advantage of ACLU in detecting internal defects.

Active infrared thermography NDT techniques are well known for enabling fast, full-field, non-contact inspections of large areas of composite materials, representing a complementary alternative to UT, as evidenced by several works comparing such NDT approaches [16,17]. Furthermore, their ability to detect delaminations in FRP materials is widely proven [18]. However, the experimental implementation of conventional IR-NDT techniques on FMLs remains limited to relatively few studies, primarily concerning GLARE [17,19–22]. In general, optically excited techniques such as Pulsed Thermography and Lock-In Thermography have limited probing depth due to the high thermal diffusivity of the aluminium facing, which acts as a fast heat sink.

Active thermography approaches have also been used to inspect FML panels. Bu et al. [17] investigated a 5-layer GLARE panel with flat-bottom-holed (FBH) defects using a long-pulse infrared thermography setup, assessing various post-process algorithms to enhance the signal-to-noise ratio of the resulting image. FBHs with defects below 6 mm in diameter, even if sub-cortical, remained hard to detect due to thermal diffusivity differences and lateral heat diffusion.

In [18], the capability of three IR-NDT techniques, namely pulsed, frequency modulated, and flying laser thermography, is demonstrated to characterize interlaminar delamination in GLARE, while in [19], with the aim of numerical analyses, the possibility of laser thermography in inspecting other types of FMLs are explored. Song et al. [20] used laser thermography and laser ultrasound on artificial CFRP disbonds, with different sizes and depths, providing a solution for high-efficiency imaging of subsurface defects in CFRP composites with high detectability.

In the UT inspection fields, the most promising NDT technique for scanning FMLs is the Laser Ultrasonic Testing (LUT). LUT is a non-contact, NDT technique that uses a laser to generate and acquire ultrasonic waves in materials and detect internal defects, delamination, and thickness variations [21]. This method has the benefits of combining the flexibility and precision of laser systems, enhancing the effectiveness of UT for inspecting complex geometries, high-temperature environments, and materials where traditional contact methods are challenging.

In LUT, a high-power pulsed laser is used to generate ultrasonics by inducing rapid thermal expansion or ablation on the surface of a material. These waves propagate through the material and interact with internal features such as cracks, voids, inclusions, and delamination. A separate laser interferometer is then used to detect the nanometric surface displacement produced by the returning ultrasonic waves.

Since LUT does not require physical contact or a coupling medium, it is ideal for remote, automated, and high-speed inspections, especially in industries such as aerospace, automotive, and power generation. It is particularly useful for testing composite materials, thin sheets, and curved surfaces, where conventional probes are less effective. The LUT technique has gained considerable attention in recent years, especially for the inspection of complex materials such as FML and other composite structures. LUT offers several advantages over traditional contact-based testing, including non-contact methods, high spatial resolution, wide frequency bandwidth, and the ability to inspect complex geometries.

For FMLs, laser ultrasound is highly effective in detecting delamination between metal and composite layers, characterizing the fiber–matrix interface, and also assessing impact damage and fatigue-induced degradation. The application of the Laser UT technique also has limitations. Laser devices for generation (the pulsed laser) and reception (the interferometer) are expensive and require specialized personnel to operate and interpret the ultrasonic signal. Other limitations arise from the surface finishing of the specimen, and particularly its emissivity. Specifically, the optimal setup will be a trade-off between the intensity of the acquired and generated UT waves. This phenomenon is caused by the different emissivity requirements for the generation and reception of the ultrasonic signal: low-emissivity (rough) surfaces facilitate wave generation, while high-emissivity (polished) surfaces facilitate signal reception by the interferometer.

In [22], Fattahi et al. used Lamb wave propagation to detect delamination defects in fiber-metal laminates by using contact transducers. The phase velocity of the S_0 wave offers higher sensitivity to delamination detection, while the A_0 phase velocity is better used to determine defect size. Nardi et al. [23] demonstrated that water-coupled UT has a high effectiveness in detecting gaps and overlaps on GLARE panels, both in position, shape, width, and severity; the optical inspections confirmed the accuracy of the proposed NDT.

Even inclusion defects and impact damage of CFRP and 3D printing reinforced composites can be detected by using ultrasonic phased array technology, estimating their position, size, and morphology [24]. Accurate detection and evaluation of carbon fiber honeycomb sandwich composites for aviation applications can be achieved by using a high-sensitivity non-contact Air-Coupled Ultrasonic detection system, according to Li et al. [25] and Chang et al. [26]. Cheng et al. [27] used ultrasonic waves generated by phased array laser in a coating/substrate (Ni/Al) structure. The technique proved to be effective, but it uses a PZT transducer as a detection tool. Thus, it is not a fully non-contact technique. Yang et al. [28] proposed a technique based on all-optical laser ultrasonics characterization of sub-mm layers in a multilayer structure. A limitation of this approach is that it requires a double sides access to the object being inspected.

In this paper, a 10-layer Ti-Gr FML with embedded artificial defects was manufactured and adopted as a benchmark for assessing the

performance of a pitch-catch LUT scanning technique. The outcomes of LUT are then validated and compared with a more conventional Pulsed Thermography (PT) approach.

The use of pulsed thermography for non-destructive evaluation is a common practice for advanced composites, such as CFRP [29,30] and fiber metal laminates, since the expected damage for these materials (debonding, delamination, cracking, and barely visible damage) can be detected in a reliable, accurate and rapid way [17,31]. Moreover, such a technique can quantify the extent of damage, and the costs are very competitive with respect to X-ray techniques (radiography, tomography), which also involve significant safety concerns.

Being also a well-consolidated technique for defect and damage detection in the aerospace composites [32], it was selected as a technique for data comparison. Moreover, the choice was also made since both laser-ultrasonic and flash thermography use a single shot, are both non-contact and full-field (through C-Scan for LUT). Furthermore, one of the main characteristics of pulsed thermography is that all frequency components are contained within a single transient thermal signal [33].

To the authors' knowledge, this work represents the first documented experimental implementation of a fully non-contact laser-based UT setup for the detection and characterization of deeper interlaminar defects in a Ti-Gr FML panel.

2. Materials and methods

2.1. Titanium-Graphite manufacturing

The investigated Ti-Gr FML is composed of titanium sheets and CFRP layers alternating with a specific layup. The Ti-Gr is mainly used for high-performance military/aerospace/motorsport applications and is custom-built to fit the specific requirements; unlike the commercial GLARE, it does not yet employ standardized coded layups. Even so, the most common layup found in the literature [34–36], enhancing the Titanium-CFRP synergy, is the 10-layers $[Ti/0°/90°/0°_2]_{sym,}$ also indicated by some authors as Ti-Gr 2–6-2 [34].

The manufactured Ti-Gr panel is rectangular with external dimensions of 160 mm x 100 mm and 1.4 mm of thickness. The sample comprises 10 layers with five square inserts with 10 mm sides mimicking disbonds/delaminations located at different positions and depths (interfaces) as shown in Fig. 1. The material of the inserts is fluorinated ethylene propylene (FEP) with a negligible thickness (13 μm). Each artificial defect is coded with a capital letter from A to E.

The specimen on which the tests were performed was designed to test the LUT's capability to probe deeply embedded defects rather than characterize irregular/realistic shapes. The choice of detecting and characterizing a damaged area of only 100 mm^2 is quite challenging and, to the authors' knowledge, has no precedent in the FML NDT literature. Moreover, the square shapes allowed for testing the technique's sensitivity to resolve sharp edges along the x and y scan directions.

2.2. Laser ultrasonic experimental setup

The experimental setup for the LUT comprises a pulsed laser as a UT wave generator, a continuous wave (CW) interferometric unit to acquire the surface displacement, a motorized micrometric x-y stage for moving the sample, and an analog-to-digital board for signal acquisition.

Wideband ultrasonic waves are generated with nanosecond laser pulses in the thermoelastic regime. The laser source is an Nd:YAG emitting in the infrared spectrum with a wavelength of 1064 nm (made by Quantel laser, Lumibird group, Lannion, FRANCE; model Brilliant B), whose beam is focused on the sample surface using optics for the beam path. The UT waves are generated in the range between 1 MHz and 50 MHz with a duration of 8.5 ns. The diameter of the beam, before its focusing, is 4 mm, the maximum injectable energy is 100 mJ, while the maximum multiple shooting repetition rate is 20 Hz.

The laser receiving unit has a wavelength of 532 nm and is focused on the sample surface using a 100 mm focal length spherical lens, obtaining a circular spot of ~ 0.2 mm in diameter. The detectable bandwidth of the interferometer reaches 50 MHz. The electrical signal coming from the laser receiver is converted by an 8-bit analog–digital board, triggered by the pulsed laser, and transferred and stored by a workstation for further signal processing and visualization. The linear/raster scanning of the sample surface is performed by moving the sample with an x-y motorized micro-positioning stage (made by Thorlabs®) triggered step-by-step by the acquisition and processing software running on the desktop computer.

Both laser devices with their focusing lenses and the motorized micro-positioning stage are mounted on an optical bench (see Fig. 2b). The distance between the specimen and the generation/receiving lasers can be chosen according to the employed lenses. A schematic representation of the adopted setup is shown in Fig. 2a, while in Table 1 a

Defect	Position from top face
A	1st interface
B	2nd interface
C	3rd interface
D	4th interface
E	5th interface

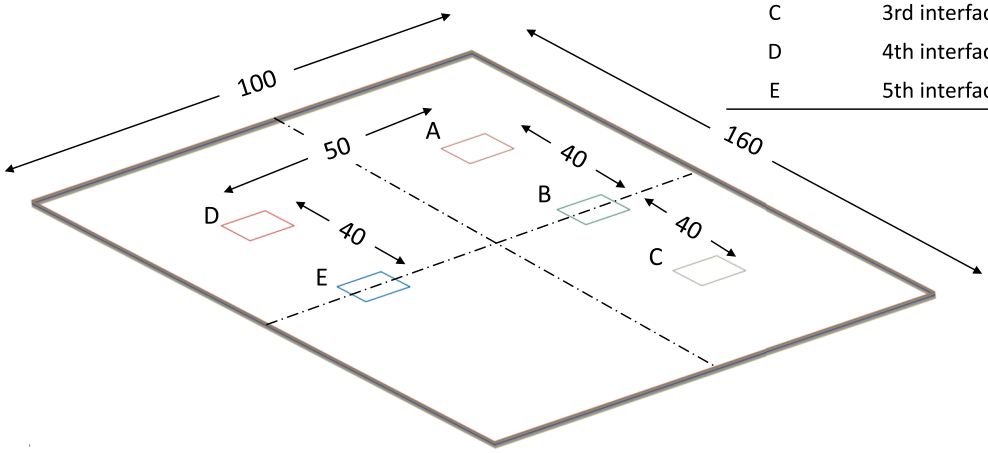

Fig. 1. Schematic representation of the Ti-Gr sample with an overall thickness of 1.4 mm. The nominal positions of the five square-shaped defects are indicated in mm.

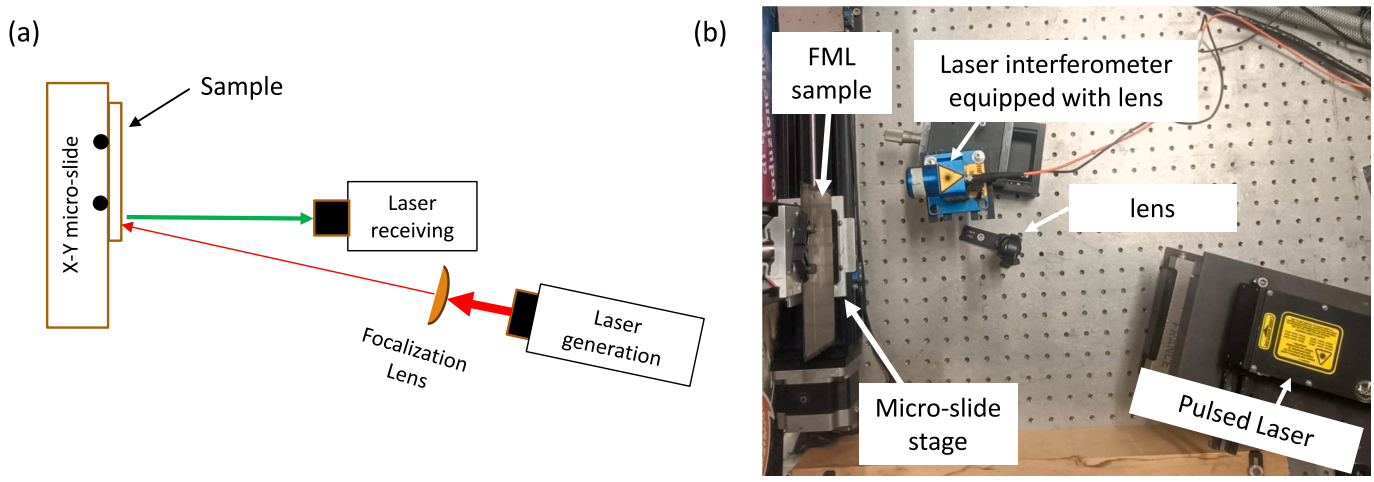

Fig. 2. Schematic representation of the experimental LUT setup (a); picture of the setup taken from the laboratory (b).

Table 1
Specification of the laser UT devices adopted in the UT setup.

Laser Generation (pulsed)	**Max energy**	**100 mJ**	**Laser Receiving (CW)**	**Power**	**1 W**
	Wavelength	1064 nm		Wavelength	532 nm
	Max frequency	20 Hz		Detection bandwidth	1 – 50 MHz
	Beam diameter	4 mm		Laser spot diameter	0.2 mm
	Pulse duration	8.5 ns		Optical stand-off	100 mm
	Optical stand-off (focusing lens)	200 mm			

specification summary of the laser devices is reported.

It is well known that often both sides of a structure are not accessible, especially in the case of box-shaped structures. For this reason, a pitch-catch configuration was chosen to generate and acquire the signals, mimicking a periodic inspection. To tune the LUT setup parameters to detect the five embedded defects (from A to E), three scanlines were used, see Fig. 3. Scanline 1 passes over a sound zone of the panel and is used to ensure the absence of any false positives during the calibration. Defects A, B, and C are inspected by scanline 2, while defects D and E are inspected by scanline 3. The tests were conducted on only three scan-lines to simplify the analysis and clearly demonstrate that the system is capable of detecting both the presence and the absence of defects. It is also necessary to perform a higher number of scans and to space them closer together to ensure complete coverage of the specimen and to detect even defects smaller than the current scanline spacing. Outcomes from each scanline are then summarized and visualized in a B-scan map by acquiring the A-scan signals in steps of 2 mm.

Once the defects have been detected using the B-scan visualization, a refined C-scan in steps of 1 mm is performed in the region of interest around each defect to characterize the boundaries.

2.3. Theoretical background: Multi-signal homodyne interferometry

A laser beam reflected by a rough sample surface generates many optical speckles. In a speckle-based measurement system, this beam is combined with a reference beam from an interferometer and focused onto an array of photodetectors. Each detector in the array captures several speckles and generates a homodyne signal. These detectors

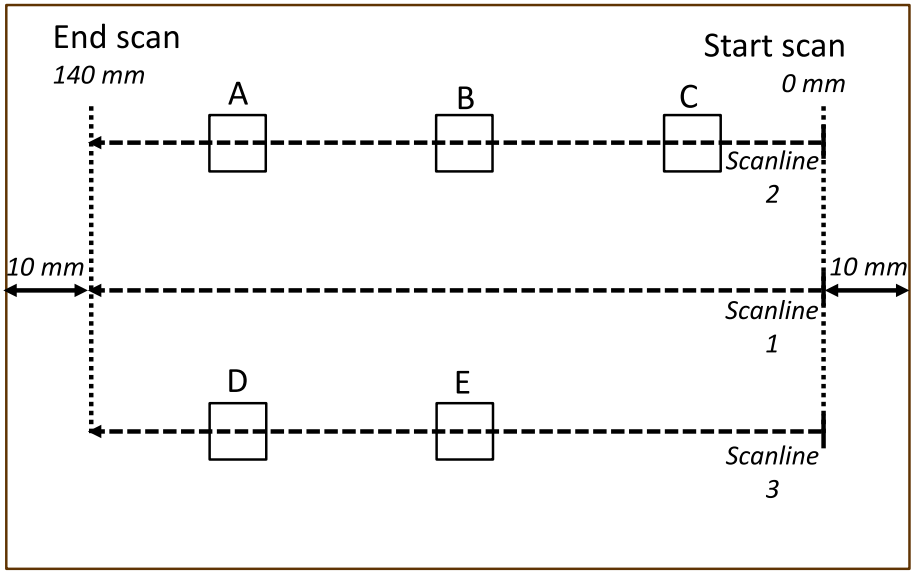

Fig. 3. Scanlines adopted for the B-scan. Scanline 1 passes over a sound zone while scanlines 2 and 3 pass over the nominal defect position.

output an analog voltage that varies over time, corresponding to the rectified instantaneous displacement of the surface at ultrasonic frequencies.

In our equipment, a speckle-based interferometer with a fifty-element photodetector array is used. This setup enables the detection of ultrasonic waves across different environments while minimizing sensitivity loss on rough surfaces. Fig. 4 illustrates the operating principle of the device. A laser beam produced by the internal laser source travels through several optical components before being focused into a multimode optical fiber. Approximately 4—5% of the beam is naturally reflected toward the receiver at the fiber's input, while the remainder is directed onto the sample. The scattered light from the sample is collected by a large lens on the front of the optical head, which maximizes the number of speckles for signal analysis. This speckled light is then guided back through the fibre and interferes with the 4—5% of the light that was initially reflected. As it travels back through the multimode fibre, the light's polarization components become scrambled. Once inside the system again, the beam passes through a Polarized Beam Splitter (PBS), which filters out the vertical polarization component and sends it to one of the two detector arrays. The remaining light moves through an Optical Isolator (containing a Faraday rotator and a second PBS), which redirects the now-vertical polarization component (originally horizontal) to the second multi-channel detector. Each homodyne signal is processed in parallel using a random quadrature demodulation approach, which leverages the inherent randomness of the speckle phase distribution. Due to this random phase behavior across all fifty detector channels, the system is built to rectify signals without relying on phase alignment. This electronic processing design enables single-shot measurements of fast-moving objects through rectified demodulation filtering. As a result, signal noise is reduced, and the system can detect nanometric displacements at high frequencies more effectively.

2.4. Laser ultrasonic sources of error and mitigation strategies

Inevitable variability or errors appear in any inspection due to limitations of instruments, environmental conditions, and data analysis. The most stringent limitations on the instrumentation are due to the interferometer's signal-to-noise ratio's dependence on surface roughness. This correlation would result in noise variability in the signal acquired during scanning that could lower the technique's detection threshold in areas with high roughness or in the presence of deep scratches.

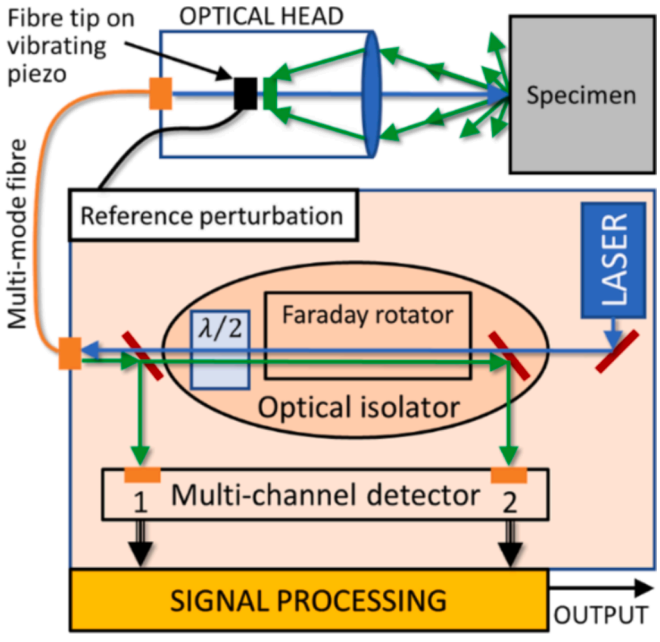

Fig. 4. Schematic representation of the laser interferometric device adopted in the LUT system 37,38.

Variations in the interferometer's signal-to-noise ratio can also arise from shifts in the laser's spot focusing due to local thickness variations or changes in panel curvature. The placement inaccuracies can also directly affect spatial measurements. Since the technique's calibration is achieved by comparing the signal acquired in defective and sound zones, systematic bias could arise if the defect footprint is not precisely recognized.

Spikes due to noise or surface scratches could mislead signal interpretation especially if direct comparison between raw single-shot A-scan acquisitions is performed. Mitigation strategies could be applied to increase the robustness of the results. Signal processing, such as filtering and averaging, enhances the signal-to-noise ratio, leveling or canceling false spikes.

The laser power source could be varied adaptively (within the same thermoelastic regime) as a function of the interferometer's signal-to-noise ratio to level the signals.

Auto-focusing devices could be easily implemented for both laser devices. The non-contact and flexible LUT setup is well-suited to be on board a robotic manipulator [39]. The latter implementation would reduce positioning errors and increase measurement repeatability.

Quick laser generation/acquisition allows for multi-scan on the same point, thus averaging reduces scattering. Implementing data fusion by combining the results of different inspection techniques (even more conventional ones) improves robustness. In this work, for example, the result of the LUT was compared with that of the PT, and both techniques could be implemented simultaneously and in parallel on board the same robotic arm.

2.5. Pulsed thermography experimental setup

In Fig. 5, the PT experimental setup is provided. A flash lamp powered by a power supply capable of providing 4800 Ws, is placed on the same side of the infrared camera.

Non-destructive evaluation by pulsed thermography was performed using a Flir Systems X8400sc cooled thermal camera, having a thermal sensitivity of 20 mK @ 30°C. Sub-windowing was set at 544 × 640 pixels with a frame rate of 150 Hz and an integration time of 602 μs. The thermal camera and the flash lamp were placed on the same side of the sample in reflection mode at a distance of 500 mm and 250 mm from the specimen, respectively. The IR camera is equipped with a MW 28 mm 2.0 HD lens, acquiring an instantaneous field of view (IFOV) of 98 microrad.

The infrared camera was focused on the sample surface, slightly tilted with respect to the sample perpendicular to avoid the narcissus effect, to acquire thermal evolution during the test.

The frame acquisition is triggered by the single pulse of the flash lamp. After the pulse, sampling is carried out on a fixed time window sufficient to normalize and homogenizethe temperature across the whole sample surface. The thermograms were post-processed using a custom script in Matlab® to extract the phase content of the acquired surface thermal evolution.

The sample surfaces were uniformly painted black. The paint was a matte paint having an emissivity of 0.95 in the mid-wave spectral range [40,41]. High emissivity paint reduces the errors due to reflected radiation and improves both the reliability and reproducibility of the thermography measurements.

In Table 2, the thermal properties of the sample components are reported.

3. Results and discussions

The outcomes of this research are based on an experimental defect signature that was found after a setup optimization that involved the fine-tuning of pulsed laser power, laser spot shape, and source-receiving

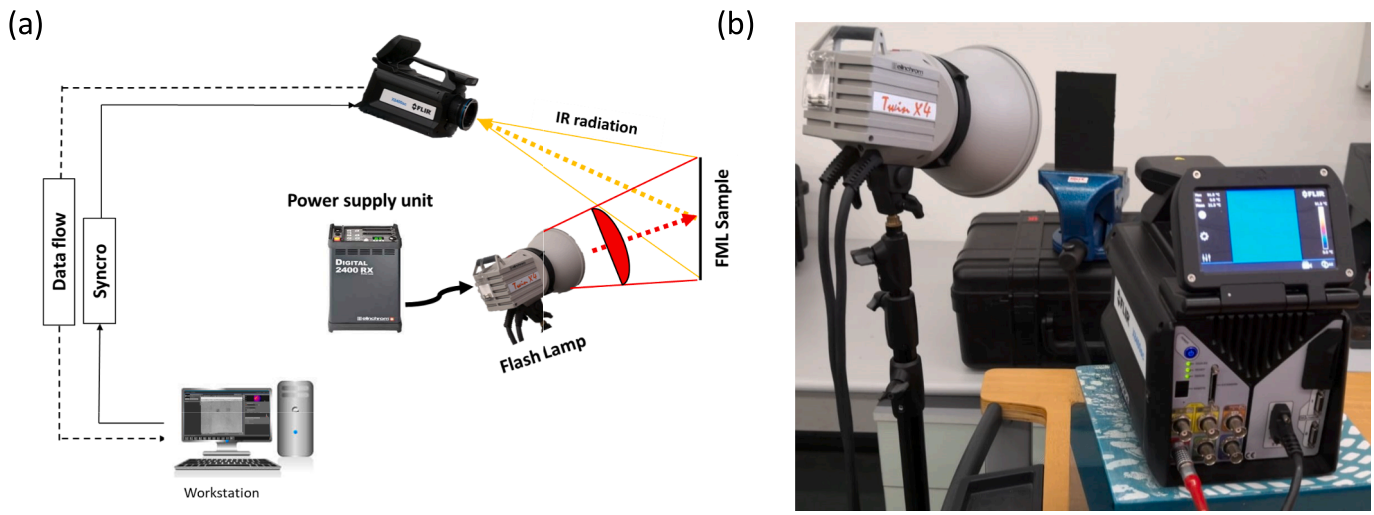

Fig. 5. Schematic representation of the experimental IRT setup (a); picture of the setup taken from the laboratory (b).

Table 2
Thermal properties and dimensions of the Ti-Gr panel components.

	FEP insert	Air	Titanium (6Al-4 V grade 5)	CFRP //	CFRP ⊥
Specific heat capacity [J/kg K]	1172	1000	500	1310	
Thermal Conductivity [W/m K]	0.195	0.026	6.7	5.65	0.35
Thickness [mm]	0.013	//	0.1	0.15	
Density [kg/m^3]	2150	1.22	4760	1600	

(S-R) distance.

Minimizing the S-R distance led to an enhanced signal-to-noise ratio, indicating that an overlap between the source and the receiving lasers could be the best solution. However, since the laser shot generates dust/surface deposit vaporization (lying on the focalspot), a shielding effect on the laser interferometer was observed. This effect causes a shaded time frame of about 2 μs immediately after the shot, which contains part of the defect signature information. For this reason, a S-R trade-off distance between 1 mm and 2 mm was adopted in this study. Small deviations to this distance (< 0.5 mm) could be present and are attributable to minor setup changes.

3.1. Laser UT – injected power effect

It's well known in the literature how the focusing shape (circular/line/array) and the laser power injected affect the UT wave propagation [42–44]. In the present work, the adopted laser power has been set below the threshold of the thermoelastic regime generation to avoid any superficial damage to the external titanium layers of the FML panel.

The best results in terms of signal-to-noise ratio have been obtained with pointwise focusing.

In Fig. 6, a sequence of A-scan signals and B-scan maps acquired over scanline 1 with gradually increased laser power is reported. All signals have been filtered to reduce noise with a first-order bandpass between 1 MHz and 2 MHz.

From the maps a peculiar trend in the energy distribution between the two wave packets is observed. Two distinct wave packets can be identified by observing the signals generated in the intermediate power range between 18.2 mJ and 19.4 mJ. The first one (the quickest) can be identified between 0.5 μs and 3 μs, while the second, resembling a slightly stretched echo of the first, is found between 3 μs and 8 μs. The amplitude of the first wave packet strongly attenuates for lower injected power (< 18.2 mJ), as can be seen in the first row of Fig. 6. At higher laser power, above 19.4 mJ, a similar attenuation is observed in the second wave packet (the echo), with an increased intensity of the first wave packet, on the contrary. It's worth noting that the first wave-packet shape remains the same regardless of the injected power, confirming that the UT generation regime does not change. In order to preserve the information contained in the UT wave, intermediate power levels (between 18 mJ and 20 mJ) have been adopted in all the acquisitions.

3.2. Laser UT – Defect detection (A-scan and B-scan)

In Fig. 7a the A-scan signals from scanlines 2 and 3 passing over the detected defects A, B, C and D are shown, while in Fig. 7b B-scans for scanlines 2 and 3 are reported. The data shown are obtained with a laser power of 19.4 mJ for the reasons detailed in section 3.1; all signals are averaged over 3 acquired values and filtered with a first-order passband between 1 MHz and 2 MHz to reduce noise and leveling spikes.

Considering the anisotropic nature of the FMLs given by the presence of numerous interfaces with different thicknesses and materials, combined with the overall small thickness of the panel, the formation of Lamb waves with scattering and mode conversion is expected. The clear discrimination of each component of the generated composite UT signals could probably be studied through specific numerical simulations of UT wave propagation in finite element modeling dynamic analyses, see [45,46], but this would require an effort that falls beyond the scope of this specific research and would be the object of further research.

Fig. 7a shows the A-scans signals for scanlines 2 and 3. By comparing a signal acquired in a sound and defective region (e.g. scanline 2 @ 20 mm and 102 mm), the defect signature can be found inside the dotted red box marked in Fig. 7a. In particular, the investigated portion of the signal is 1 μs far from the beginning of the wave (after the TOF) and has an extension of 1 μs (see Fig. 7a in the upper-left corner). In this region, a repetitive amplitude variation is observed when the scanline passes over the defect area, as also evidenced by the B-scan maps in Fig. 7b. To discriminate the presence of the defect, a threshold method was adopted, checking if the half-wave amplitude exceeds the threshold in positive OR (Boolean) negative. The positive and negative threshold values were set after the preliminary calibration with scanline 1 (for the adopted injected power 18.2 mJ), which scans sound zones only. The values are determined symmetrically to 0 and with a maximum amplitude of 0.125 V. In Fig. 7a, the dotted red box highlights how in the defect area, for both scanlines 2 and 3, at least one of the half-wave amplitudes exceeds the imposed limits, triggering the defect presence. Please note that scale limits for scanlines 2 and 3 are different, thus the

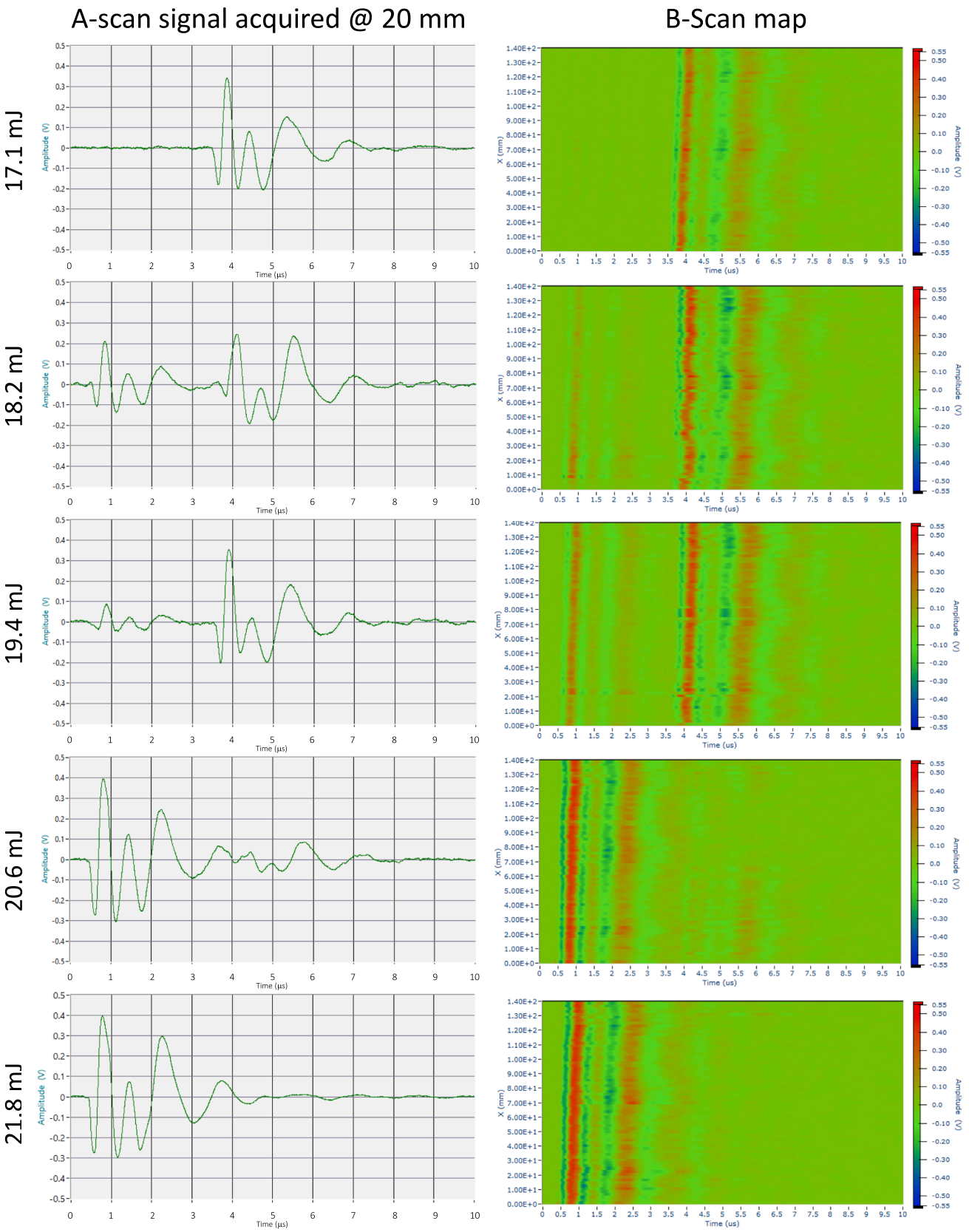

Fig. 6. A-scan signals (on the left) acquired at 20 mm distance from the scanline start and B-scan maps (on the right) for laser power levels ranging between 17.1 mJ and 21.8 mJ at fixed S-R distance on a sound zone.

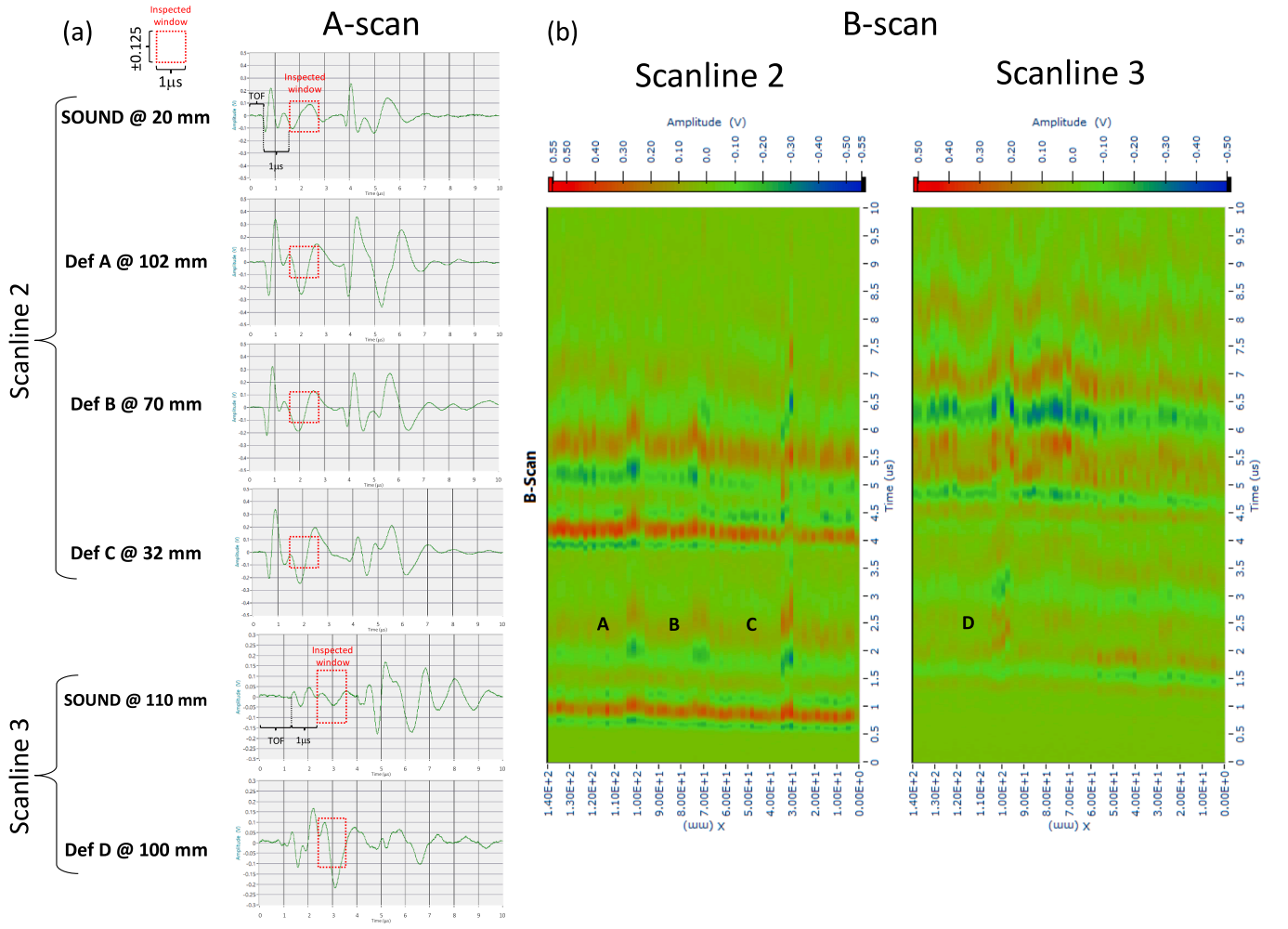

Fig. 7. A-scan signals in (a) for the four inspected defects and the relative sound zones coming from the scanline 2 (defects A, B and C) and scanline 3 (defect D); B-scan maps in (b) for the scanlines 2 and 3.

dotted box is visually stretched for scanline 3.

The B-scan map visualization in Fig. 7b confirms the detection of defects A, B, C, and D, but the overall defect contrast is lower for scanline 3 (defect D). The longer TOF reported on the scanline 3 is probably due to a slightly different S-R distance for scanline 3 (acquired in a different experimental session). Even if scanline 3 passes over defect E (as seen in Fig. 3), no clear distinction of the defect is possible.

It should be noted that defects from A to E are located at progressively deeper interfaces from the inspected surface (see Fig. 1); therefore, the difficulty in detecting defects D and E located at the fourth and fifth interfaces, respectively, was expected. The central positions of defects A, B, C, and D can be extracted from the B-scan of scanline 2 and scanline 3 and are respectively 30 mm, 70 mm, and 100 mm for A, B and C, while it is 100 mm for defect D; all the defect linear extensions have a ± 2 mm tolerance (comparable with the linear step resolution). Comparing the detected defect positions with the nominal reported in Figs. 1 and 3, a discrepancy of 10 mm (100 mm detected instead of 110 mm of the nominal) on the defect A and D positions emerges. This difference will be further explored by comparing these outcomes of the pulsed thermography (see next section 3.4).

3.3. Laser UT – Defect characterization (C-scan)

In Fig. 8, refined C-scan visualizations in the region of interest with dimensions 20 mm x 20 mm around the central position of each defect is used to characterize the boundary. Looking at the four panels of Fig. 8, the shallower defect A is well characterized with a square shape and 10 mm x 10 mm dimensions, in perfect agreement with its nominal dimensions. Defect B, located at the second interface, is slightly underestimated in terms of area with an approximate horizontal x vertical (H x V) size of 10 mm x 7 mm. Defects C and D, located at the third and fourth interfaces, are underestimated in terms of area with a blurred boundary and an approximately H x V size of 6 mm x 7 mm and 8 mm x 8 mm, respectively.

3.4. Pulsed thermography results

As mentioned, the PT is a established non-destructive evaluation setup for testing composite materials and is used as a companion technique for verifying the LUT results in terms of defect detection and characterization. It should be noted that PT is not a commonly employed technique for these specific composite materials (FML panels are typically inspected using water-coupled ultrasonic testing [13]); nonetheless, there are studies in the literature that report the use of this setup [47].

It is observed that because of the metallic facing in the material studied, a relatively high sampling time resolution is necessary to acquire the thermal wave and detect the defect signature. In this work, a relatively high frame rate of 150 Hz is used, which is about two orders of magnitude faster than the values typically employed on pure polymer and fiber-reinforced polymer materials. In the PT test, the single pulse delivers a series of thermal waves at different frequencies into the

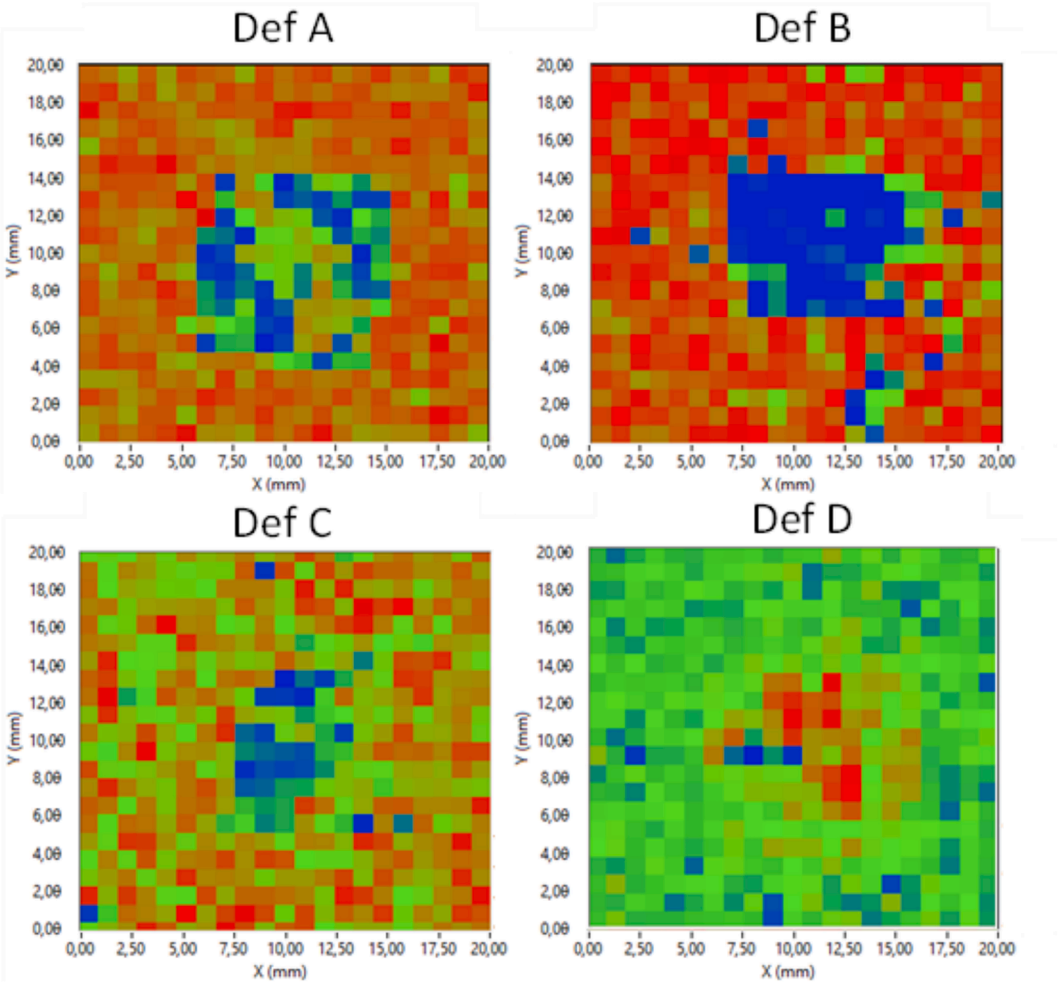

Fig. 8. Detailed C-scan maps for the four detected defects A, B, C and D located at gradually increased depth from the scanned surface.

sample. The thermal response from the sample surface, acquired over the cooling transient, is analyzed in the frequency domain by the

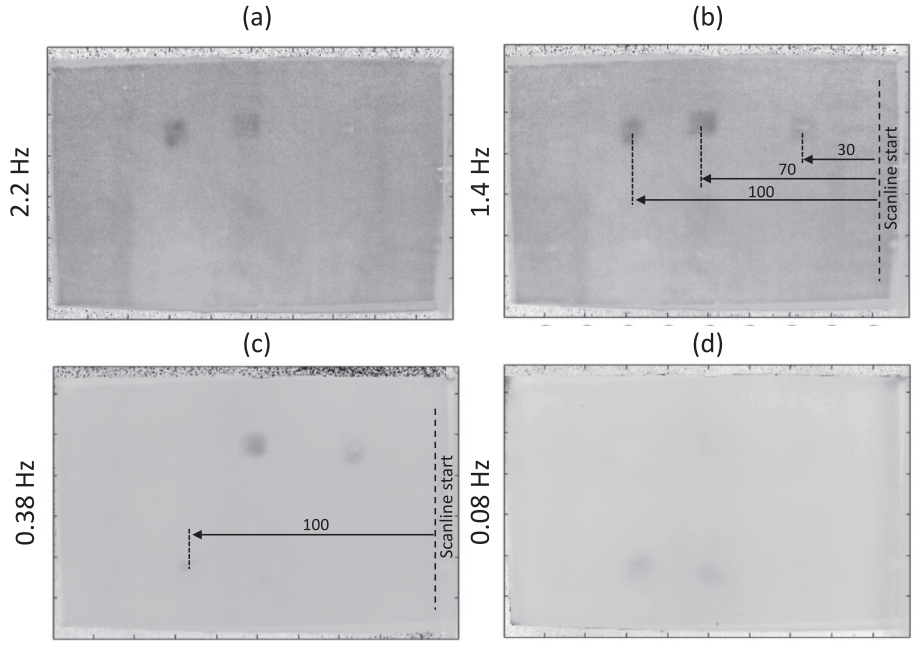

Fig. 9. PPT phasegrams extracted at different selected frequencies, detecting the 5 defects.

Discrete Fourier Transform, and the phases of the harmonic content retrieved from each analyzed point are presented in graphical form as phasegrams. This type of post-processing evaluation of pulsed thermographic data is called pulsed phase thermography (PPT).

Figure 9 shows four phasegrams obtained at selected frequency values of 2.2 Hz, 1.4 Hz, 0.38 Hz and 0.08 Hz.

It is well known in literature that high frequencies are better suited for shallower defects, while low frequencies are better suited for deeper ones [48]. This statement is supported by results shown in Fig. 9, where the phasegram at the higher frequency of 2.2 Hz generates a thermal signature for defects A and B (Fig. 9a) located at the first and second interfaces while the deeper defects D and E located at the fourth and fifth interfaces are barely detected with the lower frequency of 0.08 Hz (Fig. 9d). No clear indication of the defect borders can be retrieved deeper than the third interface (defect C).

The PPT image visualization is also used here to evaluate the actual position of defects. In Fig. 9b and c the measurements of the central positions of the 4 defects are shown, confirming what was stated with the LUT. It has been observed that two defects (A and D) have slightly shifted from their original positions. This likely occurred during the lay-up process and handling of the sample before curing.

Considering that pulsed thermography allows the detection and quantification of defects in the case of impact damage [7,49], and that FMLs are prone to such damage, which produces delamination, debonding, and intralaminar cracks, a quantitative correlation between depth and frequency has been performed.

The phasegrams were analyzed with the Color Thresholder App of Matlab using the L*a*b* color space, which allows a clear separation between luminance and chromatic information. Since the chromatic information was absent in the images (grayscale palette), the segmentation was carried out by applying thresholding only on the L* channel to highlight the edges of the defect. Using the L*a*b* colour space and adjusting only the L channel in a grayscale phasegram allows the segmentation to be performed exclusively on image lightness, independently of colour information. The L channel represents the perceptual brightness of each pixel, so thresholding is equivalent to applying an intensity-based segmentation. By selecting a range of L values, the binary mask allowed the separation of regions of interest based on how bright or dark they are, while ignoring chromatic components (a* and b*). The images were also inverted, enhancing defect identification.

The correlation between defect depth and the frequency-domain phasegrams is reported in Fig. 10.

The observed correlation is well described by an exponential law, yielding a coefficient of determination (R^2) equal to 0.93.

Pulsed thermography can be a useful and reliable tool for assessing residual stress [50] and quantitative measurements of impact damage [29,51,52] in composites.

In this research, pulsed phase thermography allowed the measurement of defect dimensions after image calibration. Considering that the pixel size was 25 μm, the spatial resolution was accurate enough to detect the edges of each defect.

The maximum deviation from the nominal size, in terms of the largest difference between the measured value and its nominal one, has been calculated for assessing the maximum error in the thermographic measurements.

The results confirmed that for deeper defects, the detection is effective, but the evaluation of the size is not reliable. Moreover, the maximum deviation from the nominal size, in terms of largest difference between the measured value and its nominal one, has been calculated for assessing the maximum error in the thermographic measurements, which was 0.8 mm of underestimation of defect B (Table 3).

4. Conclusion

The ability of the fully non-contact Laser Ultrasonic testing and Pulsed Thermography to perform inspections of innovative hybrid composite structures, such as FMLs, is appealing to industry. The LUT setup offers flexibility for the generation of all types of UT waves, the possibility of inspecting difficult-to-access areas without requiring any surface treatment (painting), which may be necessary with thermographic techniques.

However, the intrinsically heterogeneous nature of these materials

Table 3
Defect characterization obtained with the Thermographic approach.

ID DEFECT	HORIZONTAL SIZE [MM]	VERTICAL SIZE [MM]
A	10.2	10.2
B	10.2	9.2
C	9.7	10.2
D	10.2	–
E	9.7	–

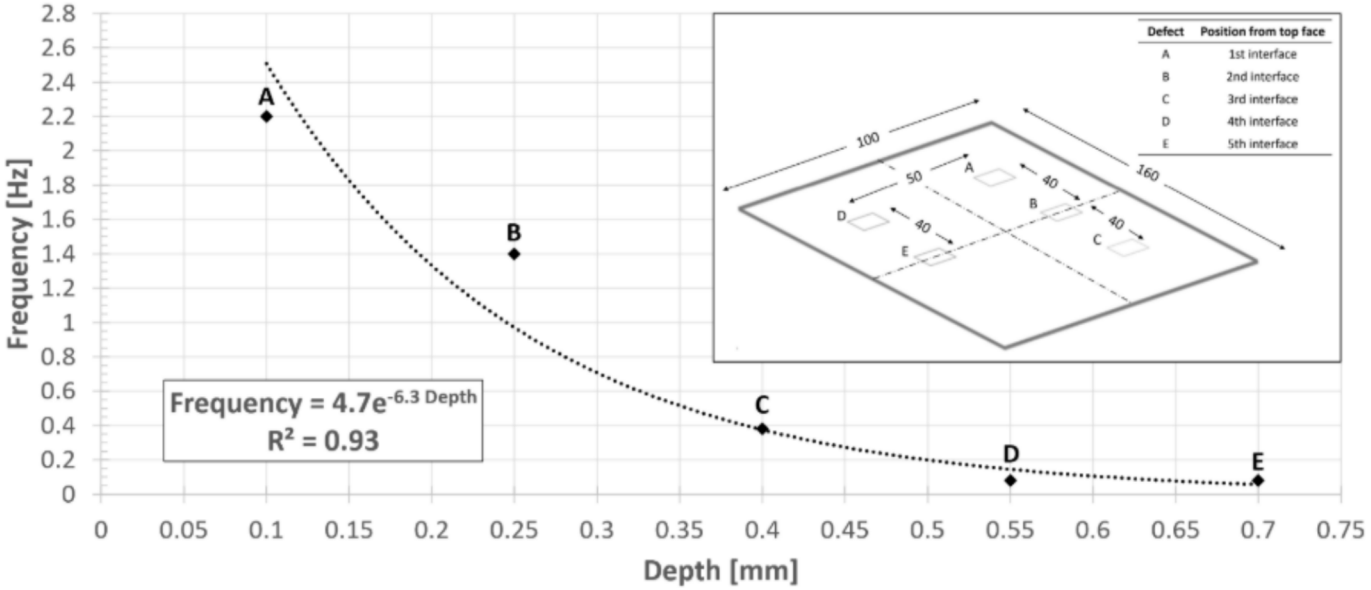

Fig. 10. Correlation between defect depth and the frequency-domain phasegrams.

makes them difficult to inspect. Due to the numerous interfaces and the different physical compositions of the layers, the generated ultrasonic waves have difficulty propagating. The analysis of the ultrasonic signal is further complicated by the formation of Lamb waves , whose interpretation and, hence, the discrimination of the defect signature become challenging.

The same inspection difficulties are encountered with the thermographic approach since high thermal diffusivity in external metal sheets makes it difficult for heat waves to probe deeply embedded interlayers, since most of the heat is conducted through the metal. For this reason, performing IR acquisition with a cooled-sensor and high-frame-rate camera is required.

A laser-laser UT setup for a fully non-contact inspection of a Ti-Gr panel with a stacking sequence $[Ti/0^\circ/90^\circ/0^\circ_2]_{sym}$, and 10 mm side squared artificial defects has been used to test the technique's capability to probe deeply embedded defects rather than characterize irregular/realistic shapes. Detecting and characterizing a damaged area of only 100 mm^2 is quite challenging and, to the author's knowledge, has no precedent in the FML NDT literature. The LUT setup has been proven to detect defects up to the fourth interface of the laminate. Due to the complexity of the acquired signal, the defect signature was found by comparing the signal in the sound and defective zones and extracting the footprint features capable of discriminating the presence of defects. The location of the defects is detected accurately, while the accuracy in estimating the extent decreases from the second interface onwards (underestimation up to 40%). The setup was developed in a pitch-catch configuration to cope with the inspection needs from only one side of the structure.

On the other hand, the PT technique was employed in reflection mode, and the setup was optimized by adjusting the relative positions of the flash, the IR-camera, and the distance to the specimen. By analyzing the results, it can be concluded that such a technique is complementary to the ultrasonic one, even though some defects are barely detected, and their edges are not clearly resolved.

This study represents, to the authors' knowledge, the first experimental application of a fully non-contact laser ultrasonic approach to the inspection of Ti–Gr fiber metal laminates. Unlike previous laser ultrasonic investigations on multilayer composites, which rely on contact receivers or require double-sided access, the proposed methodology operates in a fully optical, single-sided configuration, offering clear advantages when contact, coupling media, or rear-side accessibility are not feasible. While not intended to replace conventional state-of-the-art techniques in controlled manufacturing environments, the proposed approach is well-suited to complement existing inspection methods in realistic industrial scenarios, particularly for in-service inspections and complex geometries. By integrating the inspection method with a robotic manipulator, this approach would enable fast, remote, and detailed inline quality control of large parts.

Some drawbacks of the proposed LUT approach include the sensitivity to surface roughness, the cost of the equipment, and the need for a trade-off between laser generation and reception emissivity, since the former has better performance on matte surfaces while the latter (interferometer) on shiny ones. Moreover, a preliminary calibration on sound zones is needed to set the injected laser power, optimizing the acquired signal information.

The results obtained with the UT technique were compared and confirmed by those obtained with a more conventional pulsed thermographic technique, supporting the robustness of the proposed approach.

CRediT authorship contribution statement

Nicola Montinaro: Writing – review & editing, Writing – original draft, Visualization, Validation, Supervision, Software, Methodology, Investigation, Formal analysis, Data curation, Conceptualization. **Gabriella Epasto:** Writing – review & editing, Visualization, Investigation, Formal analysis, Data curation. **Donatella Cerniglia:** Writing – review & editing, Supervision, Investigation. **Antonio Pantano:** Writing – review & editing, Validation, Supervision.

Funding

This research did not receive any specific grant from funding agencies in the public, commercial, or not-for-profit sectors.

Declaration of competing interest

The authors declare that they have no known competing financial interests or personal relationships that could have appeared to influence the work reported in this paper.

Data availability

I have shared the link to my data

References

[1] Kirubakaran R, Kaliyamoorthy R, Munusamy R, Annamalai EB. Mechanical and vibration behavior of surface-modified titanium sheet interleaved with woven basalt/flax fiber metal laminates. Polym Compos 2023;44(12):8442–53. https://doi.org/10.1002/pc.27709.
[2] J. Sinke, «Manufacturing of GLARE Parts and Structures».
[3] «An Historic Overview of the Development of Fibre Metal Laminates».
[4] Sinmazçelik T, Avcu E, Bora MÖ, Çoban EO. A review: fibre metal laminates, background, bonding types and applied test methods. Mater Des 2011;32(7):3671–85. https://doi.org/10.1016/j.matdes.2011.03.011.
[5] Etri HE, Korkmaz ME, Gupta MK, Gunay M, Xu J. A state-of-the-art review on mechanical characteristics of different fiber metal laminates for aerospace and structural applications. Int J Adv Manuf Technol 2022;123(9–10):2965–91. https://doi.org/10.1007/s00170-022-10277-1.
[6] C. Bonavolonta, M. Valentino, N. Marrocco, e G. P. Pepe, «Eddy Current Technique Based on ${\rm HT}_{\rm c}$-SQUID and GMR Sensors for Non-Destructive Evaluation of Fiber/Metal Laminates», *IEEE Trans. Appl. Supercond.*, vol. 19, fasc. 3, pp. 808–811, giu. 2009, doi: 10.1109/tasc.2009.2019197.
[7] Montinaro N, Cerniglia D, Pitarresi G. Evaluation of interlaminar delaminations in titanium-graphite fibre metal laminates by infrared NDT techniques. NDT & E International 2018;98:134–46. https://doi.org/10.1016/j.ndteint.2018.05.004.
[8] «Delamination Detection in Fiber Metal Laminates Using Ultrasonic Wavefield Imaging», in *Conference Proceedings of the Society for Experimental Mechanics Series*, Cham: Springer International Publishing, 2022, pp. 59–72. doi: 10.1007/978-3-030-76335-0_6.
[9] «Optimization of Non-destructive Damage Detection of Hidden Damages in Fiber Metal Laminates Using X-ray Tomography and Machine Learning Algorithms», in *Lecture Notes in Networks and Systems*, Cham: Springer International Publishing, 2023, pp. 387–402. doi: 10.1007/978-3-031-16281-7_37.
[10] Smolnicki M, Duda Sz, Stabla P, Osiecki T. Mechanical investigation on interlaminar behaviour of inverse FML using acoustic emission and finite element method. Compos Struct 2022;294. https://doi.org/10.1016/j.compstruct.2022.115810.
[11] Simas Filho EF, Souza YN, Lopes JLS, Farias CTT, Albuquerque MCS. Decision support system for ultrasound inspection of fiber metal laminates using statistical signal processing and neural networks. Ultrasonics 2013;53(6):1104–11. https://doi.org/10.1016/j.ultras.2013.02.005.
[12] J. Sinke, «Some Inspection Methods for Quality Control and In-service Inspection of GLARE».
[13] W. Bisle, T. Meier, S. Mueller, e S. Rueckert, «In-Service Inspection Concept for GLARE® – An Example for the Use of New UT Array In- spection Systems».
[14] Jakubczak P, Bienias J. Non-destructive damage detection in fibre metal laminates. J Nondestr Eval 2019;38(2). https://doi.org/10.1007/s10921-019-0588-3.
[15] Wang B, et al. Non-contact detection of the interfacial microdefects in metal/CFRP hybrid composites using air-coupled laser ultrasound. Struct Health Monit 2025;24(1):243–54. https://doi.org/10.1177/14759217241234557.
[16] Palumbo D, Tamborrino R, Galietti U, Aversa P, Tatì A, Luprano VAM. Ultrasonic analysis and lock-in thermography for debonding evaluation of composite adhesive joints. NDT & E International 2016;78:1–9. https://doi.org/10.1016/j.ndteint.2015.09.001.
[17] Bu C, Liu G, Zhang X, Tang Q. Debonding defects detection of FMLs based on long pulsed infrared thermography technique. Infrared Phys Technol 2020;104:103074. https://doi.org/10.1016/j.infrared.2019.103074.
[18] Montinaro N, Cerniglia D, Pitarresi G. Detection and characterisation of disbonds on Fibre Metal Laminate hybrid composites by flying laser spot thermography. Compos B Eng 2017;108:164–73. https://doi.org/10.1016/j.compositesb.2016.09.084.
[19] Montinaro N, Cerniglia D, Pitarresi G. A numerical study on interlaminar defects characterization in fibre metal laminates with flying laser spot thermography. J Nondestr Eval 2018;37(3). https://doi.org/10.1007/s10921-018-0494-0.

[20] Song P, et al. Contactless inspection of CFRP artificial disbonds using combined laser thermography and laser ultrasonics with optical microphone. Compos Struct 2022;297:115971. https://doi.org/10.1016/j.compstruct.2022.115971.
[21] Zarei A, Pilla S. Laser ultrasonics for nondestructive testing of composite materials and structures: a review. Ultrasonics 2024;136:107163. https://doi.org/10.1016/j.ultras.2023.107163.
[22] A. Fattahi, «A guided wave propagation method for delamination detection in fiber-metal laminates», 2024.
[23] Nardi D, Abouhamzeh M, Leonard R, Sinke J. Detection and evaluation of Pre-Preg gaps and overlaps in glare laminates. Appl Compos Mater 2018;25(6):1491–507. https://doi.org/10.1007/s10443-018-9679-z.
[24] Caminero MA, García-Moreno I, Rodríguez GP, Chacón JM. Internal damage evaluation of composite structures using phased array ultrasonic technique: Impact damage assessment in CFRP and 3D printed reinforced composites. Compos B Eng 2019;165:131–42. https://doi.org/10.1016/j.compositesb.2018.11.091.
[25] Li H, Zhou Z. Detection and characterization of debonding defects in aeronautical honeycomb sandwich composites using noncontact air-coupled ultrasonic testing technique. Appl Sci 2019;9(2):283. https://doi.org/10.3390/app9020283.
[26] Chang J, Lu C, Kawashima K. Development of non-contact air coupled ultrasonic testing system for reinforced concrete structure. In: 2013 far east forum on nondestructive evaluation/testing: new technology and application. Jinan, China: IEEE; 2013. p. 197–200. https://doi.org/10.1109/fendt.2013.6635555.
[27] Cheng Q, He J, Yang S, Gu X, Huang H, Luo Y. Propagation characteristics of ultrasonic waves generated by phased array laser in coating/substrate structure. Int J Thermophys 2023;44(8):116. https://doi.org/10.1007/s10765-023-03225-y.
[28] Yang X, Zhang C, Chen C, Sun A, Ju B, Shen Q. Application of all-optical laser ultrasonics for characterization of sub-mm layers in multilayer structure. Appl Acoust 2021;182:108284. https://doi.org/10.1016/j.apacoust.2021.108284.
[29] Zhu P, et al. Enhancing resistance to low-velocity impact of electrospun-manufactured interlayer-strengthened CFRP by using infrared thermography. NDT & E International 2024;144:103083. https://doi.org/10.1016/j.ndteint.2024.103083.
[30] Antonucci V, et al. Low velocity impact response of carbon fiber laminates fabricated by pulsed infusion: a review of damage investigation and semi-empirical models validation. Prog Aerosp Sci 2016;81:26–40. https://doi.org/10.1016/j.paerosci.2015.11.002.
[31] Ciampa F, Mahmoodi P, Pinto F, Meo M. Recent advances in active infrared thermography for non-destructive testing of aerospace components. Sensors 2018;18(2):609. https://doi.org/10.3390/s18020609.
[32] E07 Committee, *Practice for Infrared Flash Thermography of Composite Panels and Repair Patches Used in Aerospace Applications*. doi: 10.1520/E2582-21.
[33] S. Marinetti, Y. A. Plotnikov, W. P. Winfree, e A. Braggiotti, «Pulse phase thermography for defect detection and visualization», presentato al Nondestructive Evaluation Techniques for Aging Infrastructures & Manufacturing, A. K. Mal, A c. di, Newport Beach, CA, gen. 1999, pp. 230–238. doi: 10.1117/12.339890.
[34] Burianek DA, Giannakopoulos AE, Spearing SM. Modeling of facesheet crack growth in titanium–graphite hybrid laminates, Part I. Eng Fract Mech 2003;70(6):775–98. https://doi.org/10.1016/S0013-7944(02)00086-3.
[35] Li E. Residual tension strength study of fatigued open-hole Titanium-Graphite hybrid composite laminates. In: *Proceedings of the AIAA*; 1998. p. 2098–105. https://doi.org/10.2514/6.1998-1960.
[36] E. Li, «Residual tension strength study of fatigued open-hole titanium-graphite hybrid composite laminates», in *39th AIAA/ASME/ASCE/AHS/ASC Structures, Structural Dynamics, and Materials Conference and Exhibit*, Long Beach,CA,U.S.A.: American Institute of Aeronautics and Astronautics, apr. 1998. doi: 10.2514/6.1998-1960.
[37] Vangi D, Gulino MS, Montinaro N, Mineo C, Cerniglia D, Epasto G. On the use of two emerging laser-based flaw-detection techniques – Considerations and practicalities. Opt Lasers Eng 2023;165. https://doi.org/10.1016/j.optlaseng.2023.107551.
[38] Tanaka K, Ohtsuka Y. Effects of surface roughness of a moving test body on laser-interferometric displacement measurements. Opt Commun 1975;14(1):110–4. https://doi.org/10.1016/0030-4018(75)90070-x.
[39] Mineo C, Montinaro N, Fustaino M, Pantano A, Cerniglia D. Fine alignment of thermographic images for robotic inspection of parts with complex geometries. Sensors 2022;22(16):6267. https://doi.org/10.3390/s22166267.
[40] Chung Y, Shrestha R, Lee S, Kim W. Thermographic inspection of internal defects in steel structures: analysis of signal processing techniques in pulsed thermography. Sensors 2020;20(21):6015. https://doi.org/10.3390/s20216015.
[41] Hernandez-Valle S, Peters K. Numerical simulation of phase images and depth reconstruction in pulsed phase thermography. Meas Sci Technol 2015;26(11):115602. https://doi.org/10.1088/0957-0233/26/11/115602.
[42] Scrubye CB, Drain LE. *Laser ultrasonics: techniques and applications*. Bristol, England; Philadelphia: A. Hilger; 1990.
[43] Davies SJ, Edwards C, Taylor GS, Palmer SB. Laser-generated ultrasound: its properties, mechanisms and multifarious applications. J Phys D Appl Phys 1993;26(3):329–48. https://doi.org/10.1088/0022-3727/26/3/001.
[44] I. C. Ume, «Parametric Studies of Laser Generated Ultrasonic Signals in Ablative Regime: Time and Frequency Domains».
[45] Cerniglia D, Pantano A, Montinaro EN. 3D simulations and experiments of guided wave propagation in adhesively bonded multi-layered structures. NDT & E International 2010;43(fasc. 6):527–35. https://doi.org/10.1016/j.ndteint.2010.05.009.
[46] Liu P, Nazirah AW, Sohn H. Numerical simulation of damage detection using laser-generated ultrasound. Ultrasonics 2016;69:248–58. https://doi.org/10.1016/j.ultras.2016.03.013.
[47] Montinaro N, Cerniglia D, Pitarresi G. Evaluation of interlaminar delaminations in titanium-graphite fibre metal laminates by infrared NDT techniques. NDT & E International 2018;98:134–46. https://doi.org/10.1016/j.ndteint.2018.05.004.
[48] Ibarra-Castanedo C, Maldague X. Pulsed phase thermography reviewed. Quantitative InfraRed Thermography Journal 2004;1(1):47–70. https://doi.org/10.3166/qirt.1.47-70.
[49] Zhu P, et al. Frequency multiplexed photothermal correlation tomography for non-destructive evaluation of manufactured materials. Int J Extrem Manuf 2025;7(3). https://doi.org/10.1088/2631-7990/ada837.
[50] Zhu P, et al. Contactless and nondestructive evaluation of residual stress distribution in modified and pure HDPE materials using a novel terahertz method and line-scan thermographic technique. Compos A Appl Sci Manuf 2024;183:108220. https://doi.org/10.1016/j.compositesa.2024.108220.
[51] Zhu P, et al. A comprehensive evaluation of the low-velocity impact behaviour of intraply hybrid flax/basalt composites using infrared thermography and terahertz time-domain spectroscopy techniques. NDT & E International 2025;154:103361. https://doi.org/10.1016/j.ndteint.2025.103361.
[52] Papa I, Manco E, Epasto G, Lopresto V, Squillace A. Impact behaviour and non destructive evaluation of 3D printed reinforced composites. Compos Struct 2022;281:115112. https://doi.org/10.1016/j.compstruct.2021.115112.